IEEE Access
Multidisciplinary | Rapid Review | Open Access Journal

Received March 13, 2019, accepted April 3, 2019, date of publication April 11, 2019, date of current version April 23, 2019.

Digital Object Identifier 10.1109/ACCESS.2019.2910304

6-DOF Multi-Constrained Adaptive Tracking Control for Noncooperative Space Target

YUHAN LIU, YUEYONG LYU, AND GUANGFU MA
Department of Control Science and Engineering, Harbin Institute of Technology, Harbin 150001, China
Corresponding author: Yueyong Lyu (lvyy@hit.edu.cn)

This work was supported by the National Natural Science Foundation of China under Grant 61673135 and Grant 61603114.

ABSTRACT This paper addresses the problem of six-degree-of-freedom (6-DOF) relative position and attitude-tracking control for noncooperative space targets subject to multiple constraints, including input and full-state constraints. First, a novel 6-DOF integrated relative motion dynamics with control command coupling is established for the final approaching stage of a rendezvous task. Second, a Barrier Lyapunov function (BLF)-based controller is developed to guarantee the relative position, attitude, and velocity constraints of the spacecraft at all times. The requirement of less restrictive initial conditions compared with the quadratic Lyapunov function is presented via a detailed theoretical analysis. Third, a novel 6-DOF integrated multi-constrained adaptive tracking control scheme is proposed to simultaneously deal with input constraints, full-state constraints, unknown disturbances, and uncertainties. In particular, a solution to the chattering phenomenon, arising from the existence of sign function, is explored in an adaptive manner. Detailed controller design procedures and rigorous theoretical proof of all related closed-loop uniform ultimate bounded (UUB) stability are provided. In addition, the numerical simulation results are also exhibited to demonstrate the effectiveness and superior control performance of the proposed control scheme.

INDEX TERMS 6-DOF spacecraft control, adaptive tracking control, full-state constraints, input constraints, noncooperative space target, on-orbit service, rendezvous and docking.

I. INTRODUCTION

On-orbit service is attracting increasing attention due to its extensive applications in space [1], including spacecraft refurbishment/refueling, large structure construction, and orbital detritus management. The basis of on-orbit servicing missions is space rendezvous and docking or capturing the service target at a near distance, which requires the knowledge of a target *a priori*. Ideally, target information, including mass, moment of inertia, and attitude information, is derived from satellite communications, or with the use of known tracking points on the target. However, most satellites which require service in orbit are noncooperative targets, meaning artificial patterns are not used for cooperative measurement, and grappling fixtures applied for the capture are not mounted on the target [2]. In other words, when the targets are noncooperative, the problem of rendezvous at a near distance becomes far more complicated as there may be insufficient or no a priori information about the motion or structure of the target. This situation presents new challenges to the modeling and control of on-orbit servicing spacecraft in such missions.

The background of this paper accounts for the problem of forcing an on-orbit servicing spacecraft, namely servicer, to approach a noncooperative target at a near distance, and simultaneously enables the CCD camera of the servicer to point to the feature point on the target. Early studies generally considered the translation and rotation motions of the servicer independently [3]–[6]. However, the relative position and attitude subsystems are highly coupled in this stage, which is primarily due to the dependence of the desired relative position and attitude tracking command on the target attitude in real time, that is, control command coupling. Hence, as opposed to the independent control strategy, it is necessary to take the coupling effect between translation and rotation motions into account to derive a systematic precise control strategy for the servicer in the final approaching stage. Various modeling and nonlinear control schemes have been carried out recently to solve this challenging problem, including adaptive fuzzy control [7], sliding mode control [8], nonlinear

The associate editor coordinating the review of this manuscript and approving it for publication was Rathinasamy Sakthivel.

optimal control [9], and model predictive control [10]. It is worth mentioning that, all of these six-degree-of-freedom (6-DOF) integrated control schemes assume that the target is cooperative, in which the translation motions are usually modeled based on C-W equation or T-H equation [11]–[13]. Nevertheless, the two equations require the orbital parameters of the target, which is not suitable in noncooperative scenarios. On the other hand, in the final approaching stage, it is no longer possible to consider the servicer and target as particles because the servicer needs to aim at a certain point on the target, especially a spinning target. Line-of-Sight (LOS) coordinate-based relative position modeling method has been put forward in recent years [14]–[17]. Compared with C-W and T-H equations, the LOS coordinate-based 6-DOF modeling method describes the relative position using only the distance and LOS angles between the servicer and target. This method is more applicable to complex space missions such as rendezvous, approaching, and capturing for noncooperative targets with spin.

Note that system constraints were not considered in the above literature. In practice, constraints are frequently encountered due to the limitations of hardware, and the violation of constraints may result in a series of potential problems (e.g., safety and reliability). One of the most general restrictions is control input constraints, namely input saturation. The existence of input constraints will result in the degradation of closed-loop control performance, or even destroy the system stability. In [18], to deal with input constraints and parameter uncertainties, Lv proposed a novel command filtered backstepping controller for 6-DOF spacecraft formation flying based on anti-windup technique. Reference [19] investigated a 6-DOF control scheme of probe hovering for an asteroid, in which a radial basis function (RBF) neural network based compensator was introduced to tackle the actuator limitations. The authors in [20] designed a 6-DOF robust state feedback saturated controller for relative position tracking and attitude synchronization problems which was incorporated with a linear compensator subsystem. In [21], in the presence of actuator misalignment, a robust adaptive integrated relative position and attitude control scheme was proposed by anti-windup technique and backstepping philosophy.

In addition to input constraints, another important consideration is state constraints. In the final approaching range, to guarantee the target always stay within the LOS cone of the CCD camera, the LOS angles should be kept in a prescribed range, which indicates that the servicer attitude error between the pointing direction and desired direction should be constrained as well. Furthermore, it is essential that the velocity and angular velocity are constrained in a secure range because any violation of velocity will lead to severe performance degradation, or even a risk of losing control. Therefore, it is of practical value to study spacecraft control with full-state constraints. Reference [22] presented a novel feedback control law to deal with attitude constraints through a repulsive potential function. Using the technique of Barrier Lyapunov Function (BLF), a distributed attitude coordinated spacecraft control schemes with attitude constraints was addressed, then the controller was improved in the case without angular velocity sensors in [23]. In [24], a model predictive controller for spacecraft rendezvous and docking problem was investigated, in which the LOS cone and thrust magnitude constraints were taken into consideration. In order to meet the need of collision avoidance of a leader-follower formation system, the LOS range and angle tracking errors were constrained by Barrier Lyapunov Function [25]. In [26], a saturated full-state constrained adaptive backstepping control scheme was proposed for a 6-DOF rendezvous and proximity mission. The aforementioned literature only considered the relative position and attitude individually, or designed controllers for them respectively.

Thus, the technical difficulties of this study are listed as follows:

1) When the target is noncooperative, how to build the 6-DOF integrated relative position and attitude dynamics without the utilization of the target's information?
2) How to consider the input constraints, relative position constraint, attitude constraint, and velocity constraint for the 6-DOF dynamic model simultaneously during the final approaching stage of a rendezvous?
3) For the 6-DOF dynamic model with input constraints, how to design the reasonable control scheme to reduce performance degradation of the closed-loop system?

By aiming at fulfilling this gap, we concentrate on developing a 6-DOF integrated relative position and attitude adaptive tracking control scheme for a noncooperative space target subject to multiple constraints during the final approaching stage of a rendezvous. Compared with the existing works, this paper contains the following contributions:

1) Compared with [7]–[10], which investigated 6-DOF control problems for cooperative space target, we establish a novel 6-DOF integrated relative position and attitude dynamic model with control command coupling for the problem of tracking a noncooperative space target in the final approaching stage through LOS coordinate-based modeling method.
2) By incorporating Barrier Lyapunov Function in the controller design, we present a basic 6-DOF integrated tracking controller to handle the relative position ad attitude motion constraints. Compared with conventional quadratic Lyapunov function, we explore the requirement of less restrictive initial conditions for our control scheme via theoretical and numerical simulation analysis.
3) Compared with [22]–[25], which only considered one or two kinds of physical constraints mentioned above, a novel 6-DOF integrated adaptive tracking controller with input and full-state constraints is proposed. An auxiliary design subsystem is incorporated to mitigate the negative impact on the closed-loop performance caused by input constraints. Furthermore, the adaptive controller output is smooth by estimating

the square of unknown constant without introducing the sign function, which practically avoids the chattering phenomenon.

The rest of this paper is organized as follows. Section II covers the mathematical model and control problem statement which includes necessary lemmas and assumptions. The Barrier Lyapunov Function based controller design with unknown disturbances, input and full-state constraints is illustrated in Section III. Section IV displays the simulations results of this paper, and Section V presents a conclusion.

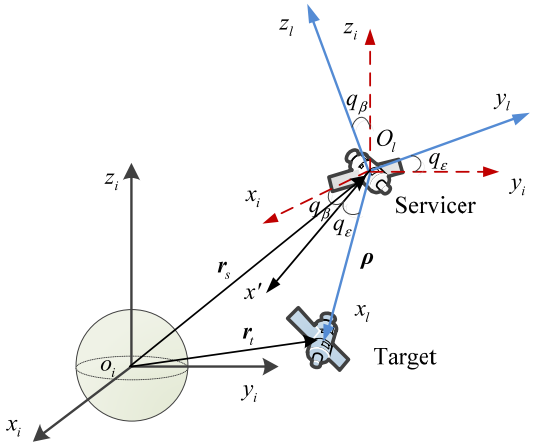

FIGURE 1. Description of LOS and inertial coordinates.

II. MATHEMATICAL MODEL AND CONTROL PROBLEM STATEMENT

A. THE DYNAMICS OF RELATIVE POSITION AND ATTITUDE

In the following, it is assumed that the servicer and the target are all rigid body, and there is no maneuvering acceleration on the target. As depicted in Fig. 1, to demonstrate the relative position relationship between the servicer and target, two principal coordinate frames are defined as follows: (1) $C_i = \{X_i, Y_i, Z_i\}^{\mathrm{T}}$ is the inertial coordinate frame whose origin is the earth; (2) $C_l = \{x_l, y_l, z_l\}^{\mathrm{T}}$ is a moving coordinate which is attached to the servicer with the line of sight $o_l x_l$ pointing to the target, $o_l y_l$ located in the plane composed by the axis x_l and y_i, and is perpendicular to the axis x_l, and $x_l - y_l - z_l$ forms a right hand frame. The sight-line deflection and inclination are defined as $q_\beta \in (-\pi, \pi)$ and $q_\varepsilon \in (-\pi/2, \pi/2)$, respectively.

The orbital equations of motion for the target and servicer are:

$$\ddot{\boldsymbol{r}}_t = -\frac{\mu}{\|\boldsymbol{r}_t\|^3}\boldsymbol{r}_t, \quad \ddot{\boldsymbol{r}}_s = -\frac{\mu}{\|\boldsymbol{r}_s\|^3}\boldsymbol{r}_s + \boldsymbol{a}_s \tag{1}$$

where $\boldsymbol{r}_t$ and $\boldsymbol{r}_s$ are the position vector of the target and servicer, respectively, $\|\cdot\|$ denotes the 2-norm of vector, μ is the earth gravitational parameter, and $\boldsymbol{a}_s$ represents the control acceleration of the servicer. Defining $\boldsymbol{\rho}$ is the relative position vector between the target and servicer, then from (1), the following formula can be obtained:

$$\frac{\mathrm{d}^2\boldsymbol{\rho}}{\mathrm{d}t^2} = \Delta\boldsymbol{g} - \boldsymbol{a}_s \tag{2}$$

where $\Delta\boldsymbol{g} = -\left(\mu/\|\boldsymbol{r}_t\|^3\right)\boldsymbol{r}_t + \left(\mu/\|\boldsymbol{r}_s\|^3\right)\boldsymbol{r}_s \in \mathbb{R}^3$. The left hand side of (2) can be rewritten as:

$$\frac{\mathrm{d}^2\boldsymbol{\rho}}{\mathrm{d}t^2} = \frac{\delta^2\boldsymbol{\rho}}{\delta t^2} + \dot{\boldsymbol{\omega}}_l^{\times}\boldsymbol{\rho} + 2\boldsymbol{\omega}_l^{\times}\frac{\delta\boldsymbol{\rho}}{\delta t} + \boldsymbol{\omega}_l^{\times}\boldsymbol{\omega}_l^{\times}\boldsymbol{\rho} \tag{3}$$

where $\delta/\delta t$ denotes the relative derivative with respect to C_l, $\boldsymbol{\omega}_l$ is the angular velocity of C_l relative to C_i, and $\times$ is the cross product operator. Let ρ be the LOS range, then according to the transformation relation between coordinate frames, we have:

$$\begin{aligned}
\boldsymbol{\rho} &= [\rho \;\; 0 \;\; 0]^{\mathrm{T}} \\
\boldsymbol{\omega}_l &= [\dot{q}_\beta \sin q_\varepsilon \;\; \dot{q}_\beta \cos q_\varepsilon \;\; \dot{q}_\varepsilon]^{\mathrm{T}} \\
\dot{\boldsymbol{\omega}}_l &= [\ddot{q}_\beta \sin q_\varepsilon + \dot{q}_\beta \dot{q}_\varepsilon \cos q_\varepsilon \;\; \ddot{q}_\beta \cos q_\varepsilon - \dot{q}_\beta \dot{q}_\varepsilon \sin q_\varepsilon \;\; \ddot{q}_\varepsilon]^{\mathrm{T}}
\end{aligned} \tag{4}$$

Substituting (4) into (3) leads to:

$$\begin{aligned}
&\frac{\delta^2\boldsymbol{\rho}}{\delta t^2} + \dot{\boldsymbol{\omega}}_l^{\times}\boldsymbol{\rho} + 2\boldsymbol{\omega}_l^{\times}\frac{\delta\boldsymbol{\rho}}{\delta t} + \boldsymbol{\omega}_l^{\times}\boldsymbol{\omega}_l^{\times}\boldsymbol{\rho} \\
&= \begin{bmatrix} \ddot{\rho} - \rho\left(\dot{q}_\varepsilon^2 + \dot{q}_\beta^2\cos^2 q_\varepsilon\right) \\ \rho\ddot{q}_\varepsilon + 2\dot{\rho}\dot{q}_\varepsilon + \rho\dot{q}_\beta^2 \sin q_\varepsilon \cos q_\varepsilon \\ -\rho\ddot{q}_\beta \cos q_\varepsilon + 2\rho\dot{q}_\beta\dot{q}_\varepsilon \sin q_\varepsilon - 2\dot{\rho}\dot{q}_\beta \cos q_\varepsilon \end{bmatrix}
\end{aligned} \tag{5}$$

In other words, by combining (2) and (5), and considering the disturbance acceleration acting on the servicer $\boldsymbol{a}_d = [a_{dx}, \; a_{dy}, \; a_{dz}]^{\mathrm{T}}$, the nonlinear relative position dynamics of the servicer and the target with respect to C_l is given as:

$$\begin{cases}
\ddot{\rho} - \rho\left(\dot{q}_\varepsilon^2 + \dot{q}_\beta^2\cos^2 q_\varepsilon\right) = \Delta g_x - a_{sx} + a_{dx} \\
\rho\ddot{q}_\varepsilon + 2\dot{\rho}\dot{q}_\varepsilon + \rho\dot{q}_\beta^2 \sin q_\varepsilon \cos q_\varepsilon = \Delta g_y - a_{sy} + a_{dy} \\
-\rho\ddot{q}_\beta \cos q_\varepsilon + 2\rho\dot{q}_\beta\dot{q}_\varepsilon \sin q_\varepsilon - 2\dot{\rho}\dot{q}_\beta \cos q_\varepsilon = \Delta g_z - a_{sz} + a_{dz}
\end{cases} \tag{6}$$

Remark 1: The first equation in (6) is called the longitudinal motion equation, which describes the variation of the relative distance. The second and third equations are called transverse motion equations, which describe the variation of LOS angle. The relative motion is described by the measurable distance ρ and LOS angles q_β and q_ε, which have an explicit physical interpretation and are significant in practical engineering applications.

For convenience of controller design, we define $\boldsymbol{p} = [\rho, q_\varepsilon, q_\beta]^{\mathrm{T}}$, then the dynamics (6) is rewritten into a compact affine form:

$$\ddot{\boldsymbol{p}} = \boldsymbol{f}_1(\boldsymbol{p}) + \boldsymbol{g}_1(\boldsymbol{p})(\boldsymbol{a}_s + \boldsymbol{a}_d) \tag{7}$$

The attitude dynamics and kinematics of the servicer are respectively given as

$$\boldsymbol{J}_s\dot{\boldsymbol{\omega}}_s + \boldsymbol{\omega}_s^{\times}\boldsymbol{J}_s\boldsymbol{\omega}_s = \boldsymbol{T}_s + \boldsymbol{T}_d \tag{8}$$

$$\dot{\Omega} = \boldsymbol{R}\boldsymbol{\omega}_s \tag{9}$$

where $\boldsymbol{J}_s \in \mathbb{R}^{3\times3}$ denotes the momentum of inertia, $\boldsymbol{\omega}_s \in \mathbb{R}^3$ is the projection of the servicer body angular velocity in inertia space onto the body frame, $\boldsymbol{T}_s \in \mathbb{R}^3$ and $\boldsymbol{T}_d \in \mathbb{R}^3$ serve as the control and disturbance torque for rotational

motion of attitude, $\boldsymbol{\Omega} = [\varphi, \theta, \psi]^{\mathrm{T}}$ is the three axis Euler angle, and $\boldsymbol{R}$ is described by:

$$\boldsymbol{R} = \begin{bmatrix} \cos\theta & 0 & -\sin\theta\cos\varphi \\ 0 & 1 & \sin\varphi \\ \sin\theta & 0 & \cos\theta\cos\varphi \end{bmatrix}^{-1} \tag{10}$$

The notation $\boldsymbol{a}^{\times}$ is used to describe a cross product of the vector $\boldsymbol{a} = [a_1,\ a_2,\ a_3]^{\mathrm{T}}$:

$$\boldsymbol{a}^{\times} \begin{bmatrix} 0 & -a_3 & a_2 \\ a_3 & 0 & -a_1 \\ -a_2 & a_1 & 0 \end{bmatrix}$$

B. 6-DOF INTEGRATED RELATIVE POSITION AND ATTITUDE DYNAMICS

The above relative position and attitude dynamics are independent from each other because there is no coupling effect between the motion of translation and rotation. However, while approaching a slow tumbling target at a close range, the desired attitude and relative position of the servicer changes with the variation of the target's attitude. The relative motion between the servicer and target in the final approaching stage is depicted in Fig. 2.

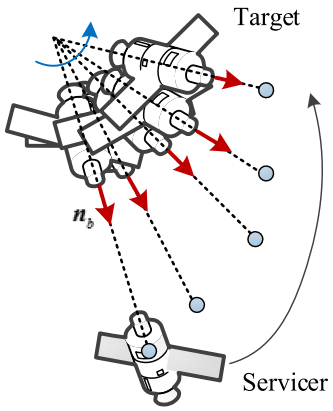

FIGURE 2. Relative motion between the servicer and target in the final approaching stage of rendezvous.

As shown in Fig. 2, $\boldsymbol{n}_b$ is defined as the direction vector of the target's characteristic point in its body frame. Hence, the desired LOS direction of the servicer is $-\boldsymbol{n}_b$. Assuming that ρ_d is the final operation distance between the servicer and target, provides:

$$\boldsymbol{\rho}_i = \begin{bmatrix} x_i & y_i & z_i \end{bmatrix}^{\mathrm{T}} = \boldsymbol{C}_i^{bt}\left(-\boldsymbol{n}_b\rho_d\right) \tag{11}$$

$$\boldsymbol{\rho}_i = \boldsymbol{C}_i^{l}\boldsymbol{\rho}_l \tag{12}$$

where $\boldsymbol{\rho}_l$ and $\boldsymbol{\rho}_i$ are the desired relative position in C_l, and its projection in C_i, $\boldsymbol{C}_i^{bt}$ and $\boldsymbol{C}_i^{l}$ are the transition matrix from the target's body frame and C_l to C_i, respectively. From the definition of C_l in Section A, C_l can be derived by rotating C_i twice with the sequence of 2-3, that is, $C_l = \boldsymbol{R}_{23}^{\mathrm{T}}$.

Then we have:

$$\begin{pmatrix} x_i \\ y_i \\ z_i \end{pmatrix} = \begin{pmatrix} \cos q_\varepsilon \cos q_\beta & \sin q_\varepsilon & -\cos q_\varepsilon \sin q_\beta \\ -\sin q_\varepsilon \cos q_\beta & \cos q_\varepsilon & \sin q_\varepsilon \sin q_\beta \\ \sin q_\beta & 0 & \cos q_\beta \end{pmatrix}^{\mathrm{T}} \times \begin{pmatrix} \rho_d \\ 0 \\ 0 \end{pmatrix} \tag{13}$$

Then the desired sight-line deflection and inclination $q_{\beta d}$ and $q_{\varepsilon d}$ can be calculated in real time by (13).

Defining $\boldsymbol{\omega}_{bt,i}$ is the projection of target's angular velocity in C_i, and is determined by

$$\boldsymbol{\omega}_{bt,i} = \boldsymbol{C}_i^{bt}\boldsymbol{\omega}_{bt} \tag{14}$$

where $\boldsymbol{\omega}_{bt}$ is the projection of the target's angular velocity which is relative to C_i in its body frame. Hence, $\dot{q}_{\beta d}$ and $\dot{q}_{\varepsilon d}$ can be calculated by

$$\dot{\boldsymbol{\rho}}_i = \begin{bmatrix} \dot{x}_i\ \dot{y}_i\ \dot{z}_i \end{bmatrix}^{\mathrm{T}} = \left(\boldsymbol{\omega}_{bt,i}\right)^{\times} \begin{bmatrix} x_i & y_i & z_i \end{bmatrix}^{\mathrm{T}} \tag{15}$$

Thus, the desire translation state $\boldsymbol{p}_d = [\rho_d, q_{\varepsilon d}, q_{\beta d}]^{\mathrm{T}}$ and $\dot{\boldsymbol{p}}_d$ can be derived.

Two assumptions are respectively made to determine the desired attitude of the servicer. First, the camera is fixed to the body frame of the servicer, with a direction of center line is coincident with the $\boldsymbol{x}_{bs}$ axis of the body frame; Second, the sunlight vector is parallel with the O_iX_i axis of C_i. To ensure the best lighting conditions, $\boldsymbol{x}_{bs}$, $\boldsymbol{z}_{bs}$, and the sunlight vector should be in the same plane. This indicates that $\boldsymbol{y}_{bs}$ is perpendicular with both $\boldsymbol{x}_{bs}$ and $\boldsymbol{\rho}_i$. Then we can obtain the desired body frame unit vectors of the servicer:

$$\boldsymbol{x}_{bsd} = \frac{\boldsymbol{\rho}_i}{\rho_d}, \boldsymbol{y}_{bsd} = \frac{\boldsymbol{\rho}_i^{\times}\hat{\boldsymbol{s}}}{\left\|\boldsymbol{\rho}_i^{\times}\hat{\boldsymbol{s}}\right\|_2}, \boldsymbol{z}_{bsd} = \boldsymbol{x}_{bsd}^{\times}\boldsymbol{y}_{bsd} \tag{16}$$

where $\hat{\boldsymbol{s}}$ denotes the projection of the sunlight vector in C_i. Then $\boldsymbol{C}_i^{bs} = \begin{bmatrix} \boldsymbol{x}_{bsd}\ \boldsymbol{y}_{bsd}\ \boldsymbol{z}_{bsd} \end{bmatrix}$ forms the transformation matrix from C_i to the body frame of the servicer. From the identical equation $\boldsymbol{C}_{bs}^{i}\boldsymbol{C}_i^{bs} = \boldsymbol{I}_3$, we can obtain the desired Euler angles $\boldsymbol{\Omega}_d = [\varphi_d\ \ \theta_d\ \ \psi_d]^{\mathrm{T}}$. Taking the derivative of (16) and combining (9), the desired angular velocity $\boldsymbol{\omega}_{sd}$ can be derived.

Remark 2. Note that $\boldsymbol{C}_i^{bt}$, $\boldsymbol{\omega}_{bt,i}$ in (12) and (14) contain the attitude information, so when the attitude of the target changes, the desired relative position will also change accordingly, which is called control command coupling.

Defining $\boldsymbol{x}_1 = [\boldsymbol{p}^{\mathrm{T}},\ \boldsymbol{\Omega}^{\mathrm{T}}]^{\mathrm{T}}$, $\boldsymbol{x}_2 = [\dot{\boldsymbol{p}}^{\mathrm{T}},\ \dot{\boldsymbol{\Omega}}^{\mathrm{T}}]^{\mathrm{T}}$, $\boldsymbol{x}_d = [\boldsymbol{p}_d^{\mathrm{T}}, \boldsymbol{\Omega}_d^{\mathrm{T}}]^{\{T}$, $\boldsymbol{e}_1 = \boldsymbol{x}_1 - \boldsymbol{x}_d = [e_\rho\ e_{q\varepsilon}\ e_{q\beta}\ e_\varphi\ e_\theta\ e_\psi]^{\mathrm{T}}$, and $\boldsymbol{e}_2 = \boldsymbol{x}_2 - \dot{\boldsymbol{x}}_d = [\dot{e}_\rho\ \dot{e}_{q\varepsilon}\ \dot{e}_{q\beta}\ \dot{e}_\varphi\ \dot{e}_\theta\ \dot{e}_\psi]^{\mathrm{T}}$, and in view of (7), (8) and (9), the 6-DOF integrated relative position and attitude error dynamics can be determined as:

$$\begin{cases} \dot{\boldsymbol{e}}_1 = \boldsymbol{e}_2 \\ \dot{\boldsymbol{e}}_2 = \boldsymbol{F}(\boldsymbol{x}) + \boldsymbol{G}(\boldsymbol{x})\boldsymbol{U} + \boldsymbol{D} \end{cases} \tag{17}$$

where $\boldsymbol{e}_1, \boldsymbol{e}_2, \boldsymbol{x}_1, \boldsymbol{x}_2 \in \mathbb{R}^6$, $\boldsymbol{F}(\boldsymbol{x})$ and $\boldsymbol{G}(\boldsymbol{x})$ are smooth, nonsingular functions, and $\boldsymbol{F}(\boldsymbol{x}) = [\boldsymbol{f}_1^{\mathrm{T}}(\boldsymbol{p}), \boldsymbol{f}_2^{\mathrm{T}}(\boldsymbol{\Omega})]^{\mathrm{T}} \in \mathbb{R}^6$. $\boldsymbol{f}_1(\cdot)$ and

$\boldsymbol{f}_2(\cdot)$ can be derived from (7)-(9), $\boldsymbol{G}(\boldsymbol{x}) = diag(\boldsymbol{g}_1, \boldsymbol{g}_2)$, $\boldsymbol{g}_1 = \text{diag}(-1, -1/\rho, 1/\rho\cos q_\varepsilon)$, $\boldsymbol{g}_2 = \boldsymbol{R}\boldsymbol{J}_s^{-1}$. $\boldsymbol{U} = \left[\boldsymbol{a}_s^{\mathrm{T}}, \boldsymbol{T}_s^{\mathrm{T}}\right]^{\mathrm{T}} \in \mathbb{R}^6$ is the control input, $\boldsymbol{D} = \boldsymbol{d} + \Delta\boldsymbol{d}$ is the unknown disturbances with $\boldsymbol{d} = \boldsymbol{G}\left[\boldsymbol{a}_d^{\mathrm{T}}, \boldsymbol{T}_d^{\mathrm{T}}\right]^{\mathrm{T}}$, and $\Delta\boldsymbol{d}$ includes model uncertainties, the second order derivatives of desired states and disturbances caused by actuator misalignment.

Remark 3. It is worth mentioning that the control gain matrix $\boldsymbol{G} = \text{diag}(\boldsymbol{g}_1,\ \boldsymbol{g}_2)$ is invertible. The singularity points of $\boldsymbol{g}_1$ are $\rho = 0$ and $q_\varepsilon = \pm\pi/2$, which can be avoided through appropriate mission design. In addition, the singularity of $\boldsymbol{g}_2$occurs when Euler angle $\varphi = \pm\pi/2$. This situation also could be circumvented as the small-angle maneuver is enough for the final approaching stage. Moreover, the state constraints are taken into account in this paper, which can further ensure the invertibility of matrix $\boldsymbol{G}$.

C. CONTROL PROBLEM STATEMENT

In this research, a 6-DOF integrated relative position and attitude tracking control problem with multiple constraints is considered. The control objective is to design an appropriate controller to ensure that the system state $\boldsymbol{x}_1$ and $\boldsymbol{x}_2$ will converge to the desired $\boldsymbol{x}_d$ and $\dot{\boldsymbol{x}}_d$ in the presence of input constraints. In addition, the state $\boldsymbol{x}_1$ and $\boldsymbol{x}_2$ are bounded, and the full-state constraints are not violated, that is, $\forall t \geq 0$, $|x_{1i}| \leq b_{ai}$ and $|x_{2i}| \leq b_{ci} i = 1, 2, \ldots, 6$ holds. In order to achieve this control objective, following assumptions are imposed in the system (17):

Assumption 1: For the time-varying and unknown disturbance $\boldsymbol{D}$, there exists a constant $d_m \in \mathbb{R}^+$ such that $\|\boldsymbol{D}\| \leq d_m$.

Assumption 2: It is assumed that the desired state $\boldsymbol{x}_d(t)$ and its first, second order derivatives $\dot{\boldsymbol{x}}_d(t)$, $\ddot{\boldsymbol{x}}_d(t)$ are continuous and satisfy $|x_{di}| \leq A_{0i}$, $|\dot{x}_{di}| \leq A_{1i}$, and $|\ddot{x}_{di}| \leq A_{2i}$, where A_{0i}, A_{1i}, and A_{2i} are positive constants and $i = 1, 2, \ldots, 6$.

Assumption 3: There exists a positive constant g, which satisfies $0 < \|\boldsymbol{G}\| \leq g$.

III. CONTROLLER DESIGN

A. CONTROLLER DESIGN WITH FULL-STATE CONSTRAINTS

In this section, a basic controller with full-state constraints is considered. To introduce the main results of this paper, some preliminary definitions and lemmas are required.

Definition 1 [27]: For the system $\dot{x} = f(x, t)$, which is defined on an open region $\mathcal{D}$ containing the origin, a Barrier Lyapunov Function is a positive and continuous scalar function and has continuous first-order partial derivatives at every point of $\mathcal{D}$. When x approaches the bound of $\mathcal{D}$, $V(x) \to \infty$, and for $x(0) \in \mathcal{D}$, and a certain positive constant b, the solution along system $\dot{x} = f(x, t)$ satisfies $V(x(t)) \leq b,\ \forall t > 0$.

Lemma 1 [27]: For any positive constant $b_i,\ i = 1, 2, \ldots, n$ and let $Z := \{z \in \mathbb{R}^n : |z_i| < b_i, i = 1, 2, \ldots, n\} \subset \mathbb{R}^n$, $Z_i := \{z_i \in \mathbb{R} : |z_i| < b_i\} \subset \mathbb{R}, i = 1, 2, \ldots, n$, and $N := \mathbb{R}^l \times Z \to \mathbb{R}^{l+1}$ is an open set. Considering the following system

$$\dot{\eta} = h(t, \eta) \tag{18}$$

where $\eta := [w, z] \in \mathcal{N}$ is system state, $h : \mathbb{R}_+ \times \mathcal{N} \to \mathbb{R}^{l+1}$ is piecewise continuous with respect to t, locally Lipchitz with respect to z_i and uniformly continuous with respect to $\mathbb{R}_+ \times \mathcal{N}$. Assume that two positive definite functions $U : \mathbb{R}^l \to \mathbb{R}_+$ and $V_i : Z_i \to \mathbb{R}_+, i = 1, 2, \ldots, n$ exist, which are continuously differentiable in their own domains, such that

$$V_i(z_i) \to \infty \text{ as } |z_i| \to b_i \tag{19}$$

$$\gamma_1(\|w\|) \leq U(w) \leq \gamma_2(\|w\|) \tag{20}$$

where γ_1 and γ_2 are class $\mathcal{K}_\infty$ functions. Let $V(\eta) := \sum_{i=1}^{n} V_i(z_i) + U(w)$ and $z_i(0) \in \mathcal{Z}_i$. If the following inequality holds

$$\dot{V} = \frac{\partial V}{\partial \eta} h \leq 0 \tag{21}$$

then $z_i(t)$ remains in the open set $z_i \in (-b_i, b_i),\ \forall t \in [0, +\infty)$.

Lemma 2 [28]: For bound initial conditions, if there exists a continuous positive Lyapunov function $V(\boldsymbol{x})$ and class $\mathcal{K}_\infty$ functions $\pi_1, \pi_2 : \mathbb{R}^n \to \mathbb{R}$ satisfying

(1)$\pi_1(\|\boldsymbol{x}\|) \leq V(\boldsymbol{x}) \leq \pi_2(\|\boldsymbol{x}\|)$

(2)$\dot{V}(\boldsymbol{x}) \leq -c_1 V(\boldsymbol{x}) + c_2$

then the system state $x(t)$ is uniformly bounded, where c_1 and c_2 are positive constants.

Lemma 3 [29]: For any positive constant vector $\boldsymbol{k}_b \in \mathbb{R}^n$, the following inequality holds for any vector $\boldsymbol{x} \in \mathbb{R}^n$ in the interval $|\boldsymbol{x}| < \boldsymbol{k}_b$:

$$\ln \frac{\boldsymbol{k}_b^{\mathrm{T}}\boldsymbol{k}_b}{\boldsymbol{k}_b^{\mathrm{T}}\boldsymbol{k}_b - \boldsymbol{x}^{\mathrm{T}}\boldsymbol{x}} \leq \frac{\boldsymbol{x}^{\mathrm{T}}\boldsymbol{x}}{\boldsymbol{k}_b^{\mathrm{T}}\boldsymbol{k}_b - \boldsymbol{x}^{\mathrm{T}}\boldsymbol{x}} \tag{22}$$

First, for the convenience of development, the auxiliary error variables are defined as $\boldsymbol{z}_1 = \boldsymbol{e}_1, \boldsymbol{z}_2 = \boldsymbol{e}_2 - \boldsymbol{\alpha}$, where $\boldsymbol{\alpha}$ is a virtual control to be designed. Hence, the closed-loop system can be obtained as

$$\begin{cases} \dot{\boldsymbol{z}}_1 = \boldsymbol{z}_2 + \boldsymbol{\alpha} \\ \dot{\boldsymbol{z}}_2 = \boldsymbol{F}(\boldsymbol{x}) + \boldsymbol{G}(\boldsymbol{x})\boldsymbol{U} + \boldsymbol{D} - \dot{\alpha} \end{cases} \tag{23}$$

Step 1: The Barrier Lyapunov candidate is chosen as

$$V_1 = \sum_{i=1}^{6} \frac{1}{2} \ln \frac{b_{1i}^2}{b_{1i}^2 - z_{1i}^2} \tag{24}$$

where $\boldsymbol{b}_1 = \boldsymbol{b}_a - \boldsymbol{A}_0 = [b_{11}, b_{12}, \ldots, b_{16}]^{\mathrm{T}}$ is the bound of $\boldsymbol{z}_1$. It is obviously that V_1 is positive definite and continuous in the interval $|z_{1i}| \leq b_{1i}$.

The time derivative of (24) is given as:

$$\dot{V}_1 = \sum_{i=1}^{6} \frac{z_{1i}\dot{z}_{1i}}{b_{1i}^2 - z_{1i}^2} \tag{25}$$

To stabilize $\boldsymbol{z}_1$, the virtual control $\boldsymbol{\alpha}$ is designed as $\boldsymbol{\alpha} = -\boldsymbol{K}_1\boldsymbol{z}_1$, where $\boldsymbol{K}_1 = \text{diag}(k_{11}, k_{12}, \ldots, k_{16})$ is a diagonal matrix with positive constant k_{1i} as diagonal elements. Substituting (23) into (25) yields

$$\dot{V}_1 = -\sum_{i=1}^{6} \frac{k_{1i}z_{1i}^2}{b_{1i}^2 - z_{1i}^2} + \sum_{i=1}^{6} \frac{z_{1i}z_{2i}}{b_{1i}^2 - z_{1i}^2} \tag{26}$$

From (26), we can obtain that $\dot{V}_1 = -\sum_{i=1}^{6} \frac{k_{1i} z_{1i}^2}{b_{1i}^2 - z_{1i}^2} \leq 0$ holds as $z_2 = 0$, which means $z_1 \to 0$ as $t \to \infty$. The next task is to stabilize z_1 and z_2 by designing the control $\boldsymbol{U}$.

Step 2: Another Barrier Lyapunov candidate is selected as

$$V_2 = V_1 + \sum_{i=1}^{6} \frac{1}{2} \ln \frac{b_{2i}^2}{b_{2i}^2 - z_{2i}^2} \tag{27}$$

Its time derivative is

$$\dot{V}_2 = \dot{V}_1 + \sum_{i=1}^{6} \frac{z_{2i} \dot{z}_{2i}}{b_{2i}^2 - z_{2i}^2} \tag{28}$$

In order to stabilize z_1 and z_2, the ideal control $\boldsymbol{U}$ can be finally designed as

$$\boldsymbol{U} = \boldsymbol{G}^{-1} \left[-\boldsymbol{F}(\boldsymbol{x}) + \dot{\alpha} - \boldsymbol{K}_2 z_2 - \sum_{i=1}^{6} \frac{b_{2i}^2 - z_{2i}^2}{b_{1i}^2 - z_{1i}^2} z_1 - k_3 sgn(z_2) \right] \tag{29}$$

where $k_3 > d_m$. The following theorem can thus be stated as follows:

Theorem 1: Considering the 6-DOF integrated relative position and attitude system (17) with the initial conditions $z_{1i}(0) \in \Omega_{01} \in \{|z_{1i}| < b_{1i}, i = 1, 2, \ldots, 6\}$, $z_{2i}(0) \in \Omega_{02} \in \{|z_{2i}| < b_{2i}, i = 1, 2, \ldots, 6\}$, and Assumption 1 holds. The proposed controller (29) guarantees the asymptotic convergence to the desired $\boldsymbol{x}_d$, $\dot{\boldsymbol{x}}_d$ of system state $\boldsymbol{x}_1$, $\boldsymbol{x}_2$. Furthermore, for any $t \geq 0$, $|x_{1i}| \leq b_{ai}$, $|x_{2i}| \leq b_{ai}$, $i = 1, 2, \ldots, 6$ holds.

Proof: Substituting the proposed controller (29) into (28) yields

$$\dot{V}_2 = -\sum_{i=1}^{6} \frac{k_{1i} z_{1i}^2}{b_{1i}^2 - z_{1i}^2} - \sum_{i=1}^{6} \frac{k_{2i} z_{2i}^2}{b_{2i}^2 - z_{2i}^2} \leq 0 \tag{30}$$

Then according to Lemma 1, state error z_1 and z_2 will always remain in the set $|z_{1i}| < b_{1i}$ for any $t \geq 0$. Furthermore, from $\boldsymbol{x}_1 = \boldsymbol{z}_1 + \boldsymbol{x}_d$ and $\boldsymbol{x}_2 = \boldsymbol{z}_2 + \dot{\boldsymbol{x}}_d + \boldsymbol{\alpha}$, we can obtain that $|x_{1i}| < b_{1i} + A_0 b_{ai}$ and $|x_{2i}| < b_{2i} + A_{1i} + k_{1i} b_{1i} b_{ci}$ holds for any $t \geq 0$.

Integrating the above inequality (30) provides $V_2(t) \leq V_2(0)$, which means $\boldsymbol{z}_1$, $\dot{\boldsymbol{z}}_1$, $\boldsymbol{z}_2$, and $\dot{\boldsymbol{z}}_2$ are all bounded. Thus, $\ddot{V}_2$ is also bounded and $\dot{V}_2$ is uniformly continuous. From Barbalat's Lemma, it can be obtained that $z_1 \to 0$ and $z_2 \to 0$ as $t \to \infty$. Thus, Theorem 1 is proven.

Remark 4: Compared with an conventional quadratic Lyapunov function (QLF), the proposed controller based on Barrier Lyapunov Function has a less restrictive condition for initial values $z_1(0)$ and $z_2(0)$. This is explained in detail as follows.

Similar to Barrier Lyapunov method, first the quadratic Lyapunov function can be selected as

$$V_{1q} = \frac{1}{2} z_1^2 \tag{31}$$

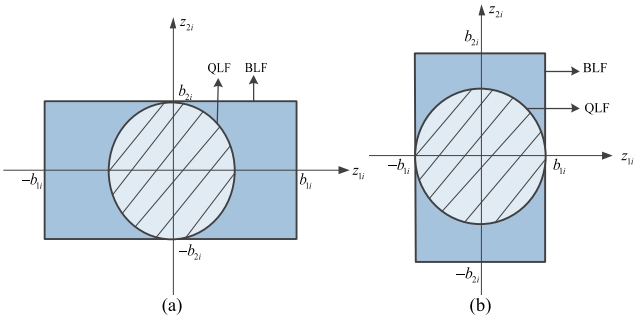

FIGURE 3. Comparison of optional initial value areas between Barrier Lyapunov and quadratic Lyapunov based methods. (a) When $|b_{1i}| > |b_{2i}|$ satisfies. (b) When $|b_{1i}| < |b_{2i}|$ satisfies.

Its time derivative is

$$\dot{V}_{1q} = z_1 \dot{z}_1 \tag{32}$$

Defining virtual control $\boldsymbol{\alpha}_q = -\boldsymbol{K}_1 z_1$, then we can obtain

$$\dot{V}_{1q} = -K_1 z_1^2 + z_1 z_2 \tag{33}$$

Selecting the second Lyapunov function as

$$V_{2q} = \frac{1}{2} z_1^2 + \frac{1}{2} z_2^2 \tag{34}$$

Then the controller can be designed as

$$\boldsymbol{U} = \boldsymbol{G}^{-1} \left[-\boldsymbol{F}(\boldsymbol{x}) + \dot{\alpha} - \boldsymbol{K}_2 z_2 - z_1 - k_3 \, sgn(z_2) \right] \tag{35}$$

Hence, the following inequality is obtained

$$\dot{V}_{2q} = -\boldsymbol{K}_1 z_1^2 - \boldsymbol{K}_2 z_2^2 \leq 0 \tag{36}$$

Integrating (30), we have $V_{2q}(t) \leq V_{2q}(0)$, which leads to $|z_1(t)| \leq \sqrt{2V_{2q}(0)}$. According to the definition of z_1 and the inequality of absolute value, we can obtain $|x_{1i}(t)| \leq |x_{di}(t)| + \sqrt{2V_{2q}(0)}$. Taking the state constraint $|x_{1i}| \leq b_{ai}$ into consideration, $|x_{di}(t)| + \sqrt{2V_{2q}(0)} \leq b_{ai}$ holds. This then provides $\sqrt{2V_{2q}(0)} \leq b_{ai} - A_{0i}$ in accordance with Assumption 2, which implies that when the following initial condition satisfies,

$$z_{1i}^2(0) + z_{2i}^2(0) \leq (b_{ai} - A_{0i})^2 = b_{1i}^2 \Theta_1 \tag{37}$$

the state constraint $|x_{1i}| \leq b_{ai}$ holds.

Similarly, it can be derived that when

$$z_{1i}^2(0) + z_{2i}^2(0) \leq (b_{ci} - A_{1i} + K_{1i} b_{1i})^2 = b_{2i}^2 \Theta_2 \tag{38}$$

$|x_{2i}| \leq b_{ci}$ holds. Taking (37) and (38) together, only when the following condition satisfies

$$z_{1i}^2(0) + z_{2i}^2(0) \in \Theta_1 \cap \Theta_2 \tag{39}$$

the full-state constraints holds. In contrast, the initial condition of Barrier Lyapunov based method is

$$\begin{aligned} |z_{1i}(0)| &\leq b_{1i} \\ |z_{2i}(0)| &\leq b_{2i} \end{aligned} \tag{40}$$

Fig. 3 illustrates (39) and (40) intuitively. The round shaded area represents the optional initial value of quadratic Lyapunov function based method, and the rectangle shaded area represents the one for Barrier Lyapunov based method.

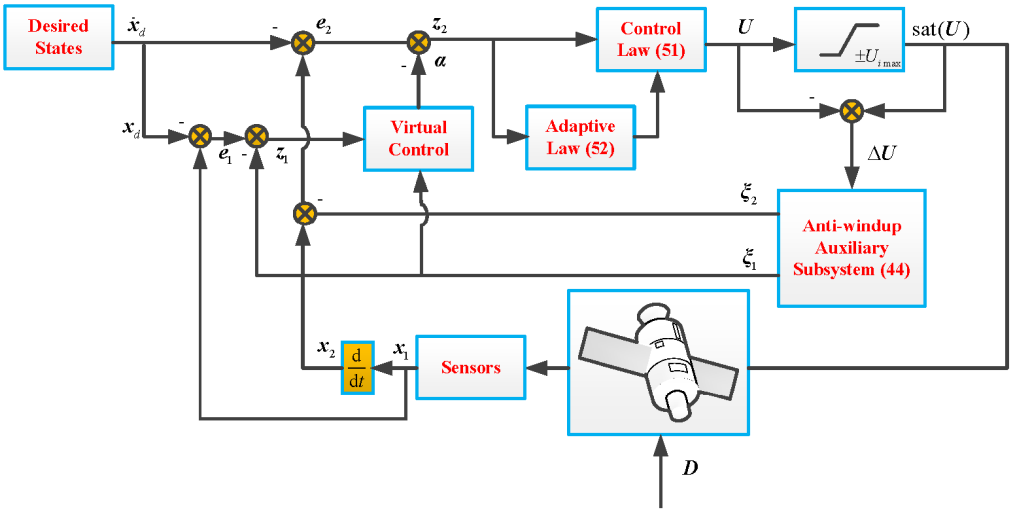

FIGURE 4. Structure of the closed-loop system.

It is clear that the Barrier Lyapunov based method has less restrictive initial conditions than the quadratic Lyapunov based method under the same state constraints, in other words, it has a broader area of optional initial value.

Remark 5: The controller proposed in (29) is able to ensure the Lyapunov stability of the closed-loop system (23) under the state constraints. However, no input saturation is taken into account, which is reasonably important for practical application. Furthermore, the constant k_3 in (29) is hard to choose because the upper bound of $\boldsymbol{D}$ is unknown. In the next section, a novel adaptive controller with input and state constraints will be presented.

B. ADAPTIVE CONTROLLER DESIGN WITH INPUT AND FULL-STATE CONSTRAINTS

The saturation of actuators can be expressed here as

$$\text{sat}(\boldsymbol{U}) = [\text{sat}(U_1), \text{sat}(U_2), \ldots, \text{sat}(U_6)]^{\mathrm{T}} \tag{41}$$

where $\text{sat}(U_i) = sgn(U_i)\min\{U_{i\max}, |U_i|\}, i = 1, 2, \ldots, 6$, $U_{i\max}$ is a known constant associated with the output capability of actuators. It is obvious that the control command $\boldsymbol{U}$ is possibly larger than the actual control input sat($\boldsymbol{U}$) provided by actuators. Hence, a difference $\Delta\boldsymbol{U}$ will exist between the desired control command and actual control input which is denoted as

$$\Delta\boldsymbol{U} = \text{sat}(\boldsymbol{U}) - \boldsymbol{U} \tag{42}$$

Assumption 4: For the control input constraints formed as (41) and (42), there exists a non-negative constant ϑ such that:

$$\|\Delta\boldsymbol{U}\| \leq \vartheta \tag{43}$$

Remark 6: Once the input constraints happens, i.e. $\Delta\boldsymbol{U} \neq 0$, the auxiliary system (44) begins to work and the excess part will be compensated by the term $\boldsymbol{C}_2\boldsymbol{\xi}_2$ in controller (51), and then $\Delta\boldsymbol{U}$ will converge to zero rapidly. Furthermore, the magnitude of $\boldsymbol{U}$ will decreases as the system states converge to the desired trajectories, which ensures that $\lim_{t\to\infty} \Delta\boldsymbol{U} = 0$. On the other hand, when control input constraints occurs, $\Delta\boldsymbol{U}$ is definitely bounded, otherwise the closed-loop system will lose control and the controller design will not make any sense. Thus, Assumption 4 is reasonable both mathematically and practically.

To attenuate the effect of input constraints, the following auxiliary subsystem is designed first on the basis of anti-windup technique:

$$\begin{cases} \dot{\xi}_1 = -\boldsymbol{C}_1\boldsymbol{\xi}_1 + \boldsymbol{\xi}_2 \\ \dot{\xi}_2 = -\boldsymbol{C}_2\boldsymbol{\xi}_2 + \boldsymbol{G}\Delta\boldsymbol{U} \end{cases} \tag{44}$$

where $\boldsymbol{C}_1$ and $\boldsymbol{C}_2$ are diagonal matrices with positive diagonal elements, $\boldsymbol{\xi}_1 = [\xi_{11}, \ldots, \xi_{16}]^{\mathrm{T}}$ and $\boldsymbol{\xi}_2 = [\xi_{21}, \ldots, \xi_{26}]^{\mathrm{T}}$ are the auxiliary subsystem output. Then the error states can be redefined as $\boldsymbol{z}_1 = \boldsymbol{e}_1 - \boldsymbol{\xi}_1$ and $\boldsymbol{z}_2 = \boldsymbol{e}_2 - \boldsymbol{\xi}_2 - \boldsymbol{\alpha}$. The closed-loop system turns into

$$\begin{cases} \dot{\boldsymbol{z}}_1 = \boldsymbol{z}_2 + \boldsymbol{\xi}_2 + \boldsymbol{\alpha} - \dot{\boldsymbol{\xi}}_1 \\ \dot{\boldsymbol{z}}_2 = \boldsymbol{F}(\boldsymbol{x}) + \boldsymbol{G}(\boldsymbol{x})\boldsymbol{U} + \boldsymbol{D} - \dot{\alpha} + \boldsymbol{C}_2\boldsymbol{\xi}_2 \end{cases} \tag{45}$$

and the block diagram of closed-loop control system is shown in Fig. 4.

Step 1: The Lyapunov candidate can be chosen as

$$V_1 = \sum_{i=1}^{6} \frac{1}{2} \ln \frac{b_{1i}^2}{b_{1i}^2 - z_{1i}^2} + \frac{1}{2}\boldsymbol{\xi}_1^{\mathrm{T}}\boldsymbol{\xi}_1 \tag{46}$$

and the time derivative of (46) is

$$\dot{V}_1 = \sum_{i=1}^{6} \frac{z_{1i}(z_{2i} + \xi_{2i} + \alpha_i - \dot{\xi}_{1i})}{b_{1i}^2 - z_{1i}^2} + \boldsymbol{\xi}_1^{\mathrm{T}}\dot{\boldsymbol{\xi}}_1 \tag{47}$$

According to (47), the virtual control $\boldsymbol{\alpha}$ is denoted as $\boldsymbol{\alpha} = -\boldsymbol{K}_1 z_1 - \boldsymbol{C}_1 \boldsymbol{\xi}_1$. Substituting (44) into (47) yields

$$\begin{aligned}\dot{V}_1 &= \sum_{i=1}^{6} \frac{z_{1i}(z_{2i} - K_{1i} z_{1i})}{b_{1i}^2 - z_{1i}^2} - \boldsymbol{\xi}_1^{\mathrm{T}} \boldsymbol{C}_1 \boldsymbol{\xi}_1 + \boldsymbol{\xi}_1^{\mathrm{T}} \boldsymbol{\xi}_2 \\ &\leq -\sum_{i=1}^{6} \frac{k_{1i} z_{1i}^2}{b_{1i}^2 - z_{1i}^2} + \sum_{i=1}^{6} \frac{z_{1i} z_{2i}}{b_{1i}^2 - z_{1i}^2} \\ &\quad - \boldsymbol{\xi}_1^{\mathrm{T}} \boldsymbol{C}_1 \boldsymbol{\xi}_1 + \frac{1}{2} \boldsymbol{\xi}_1^{\mathrm{T}} \boldsymbol{\xi}_1 + \frac{1}{2} \boldsymbol{\xi}_2^{\mathrm{T}} \boldsymbol{\xi}_2 \\ &\leq -\sum_{i=1}^{6} \frac{k_{1i} z_{1i}^2}{b_{1i}^2 - z_{1i}^2} + \sum_{i=1}^{6} \frac{z_{1i} z_{2i}}{b_{1i}^2 - z_{1i}^2} - \bar{C}_1 \left\| \boldsymbol{\xi}_1 \right\|^2 + \frac{1}{2} \boldsymbol{\xi}_2^{\mathrm{T}} \boldsymbol{\xi}_2 \end{aligned} \tag{48}$$

where $\bar{C}_1 = \lambda_{\min}(\boldsymbol{C}_1) - 1/2 > 0$.

For the purpose of dealing with unknown disturbance, uncertainties, and preventing unnecessary chattering caused by sign function, an adaptive law is designed here to estimate the square of unknown upper bound d_m, which is inspired by [30]. The estimation error is denoted as $\tilde{\kappa} = \kappa - \hat{\kappa}$, where $\kappa = d_m^2$.

Step 2: Another Lyapunov candidate can be selected as

$$V_2 = V_1 + \sum_{i=1}^{6} \frac{1}{2} \ln \frac{b_{2i}^2}{b_{2i}^2 - z_{2i}^2} + \frac{1}{2} \boldsymbol{\xi}_2^{\mathrm{T}} \boldsymbol{\xi}_2 + \frac{1}{2\gamma_0} \tilde{\kappa}^2 \tag{49}$$

where γ_0 is a positive constant to be designed.

Taking time derivative of (49) yields

$$\dot{V}_2 = \dot{V}_1 + \sum_{i=1}^{6} \frac{z_{2i} \dot{z}_{2i}}{b_{2i}^2 - z_{2i}^2} + \boldsymbol{\xi}_2^{\mathrm{T}} \dot{\boldsymbol{\xi}}_2 - \frac{1}{\gamma_0} \tilde{\kappa} \dot{\hat{\kappa}} \tag{50}$$

Thus, the controller and adaptive law are designed as

$$\begin{aligned}\boldsymbol{U} &= \boldsymbol{G}^{-1} \\ &\quad \times \left[-\boldsymbol{F}(\boldsymbol{x}) + \dot{\alpha} - \boldsymbol{K}_2 z_2 - \boldsymbol{C}_2 \boldsymbol{\xi}_2 - \sum_{i=1}^{6} \frac{b_{2i}^2 - z_{2i}^2}{b_{1i}^2 - z_{1i}^2} z_1 - \frac{\hat{\kappa} z_2}{2\varepsilon^2} \right] \end{aligned} \tag{51}$$

$$\dot{\hat{\kappa}} = \gamma_0 \sum_{i=1}^{6} \frac{z_{2i}^2 / 2\varepsilon^2}{b_{2i}^2 - z_{2i}^2} - \gamma_0 \gamma_1 \hat{\kappa} \tag{52}$$

where ε, γ_1, and β_1 are all positive constants.

Theorem 2: Considering the 6-DOF integrated relative position and attitude system (17) satisfies Assumption 1-4, and the initial conditions satisfy $z_{1i}(0) \in \Omega_{01}\{|z_{1i}| < b_{1i}, i = 1, \ldots, 6\}$ and $z_{2i}(0) \in \Omega_{02}\{|z_{2i}| < b_{2i}, i = 1, \ldots, 6\}$. Under the proposed controller (51) and adaptive law (52), the closed-loop signals $z_1, z_2, \tilde{\kappa}, \boldsymbol{\xi}_1, \boldsymbol{\xi}_2$ are uniformly bounded. Furthermore, the state error z_1, z_2 ultimately converge to corresponding compact sets Ω_{z1} and Ω_{z2}, which are defined as

$$\begin{aligned}\Omega_{z1}\{|z_{1i}| &\leq b_{1i} \sqrt{1 - e^{-2(V_2(0) + C/\beta)}}, \\ &\quad i = 1, \ldots, 6\} \sqrt{b^2 - 4ac} \end{aligned} \tag{53}$$

$$\Omega_{z2}\{|z_{2i}| \leq b_{2i} \sqrt{1 - e^{-2(V_2(0) + C/\beta)}} \tag{54}$$

Proof: Substituting (51) and (52) into (50), and considering (44) yields

$$\begin{aligned}\dot{V}_2 &= -\sum_{i=1}^{6} \frac{k_{1i} z_{1i}^2}{b_{1i}^2 - z_{1i}^2} - \sum_{i=1}^{6} \frac{k_{2i} z_{2i}^2}{b_{2i}^2 - z_{2i}^2} \\ &\quad + \sum_{i=1}^{6} \frac{z_2 \boldsymbol{I}_i \left(\boldsymbol{D} - \hat{\kappa} z_2 / 2\varepsilon^2 \right)}{b_{2i}^2 - z_{2i}^2} \\ &\quad - \bar{C}_1 \left\| \boldsymbol{\xi}_1 \right\|^2 + \frac{1}{2} \boldsymbol{\xi}_2^{\mathrm{T}} \boldsymbol{\xi}_2 - \boldsymbol{\xi}_2^{\mathrm{T}} \boldsymbol{C}_2 \boldsymbol{\xi}_2 + \boldsymbol{\xi}_2^{\mathrm{T}} \boldsymbol{G} \Delta \boldsymbol{U} \\ &\quad - \frac{1}{\gamma_0} \tilde{\kappa} \left(\gamma_0 \sum_{i=1}^{6} \frac{z_{2i}^2 / 2\varepsilon^2}{b_{2i}^2 - z_{2i}^2} - \gamma_0 \gamma_1 \hat{\kappa} \right) \\ &\leq -\sum_{i=1}^{6} \frac{k_{1i} z_{1i}^2}{b_{1i}^2 - z_{1i}^2} - \sum_{i=1}^{6} \frac{k_{2i} z_{2i}^2}{b_{2i}^2 - z_{2i}^2} \\ &\quad + \sum_{i=1}^{6} \frac{\| z_{2i} \| d_m - \hat{\kappa} z_{2i}^2 / 2\varepsilon^2 + \tilde{\kappa} z_{2i}^2 / 2\varepsilon^2}{b_{2i}^2 - z_{2i}^2} - \bar{C}_1 \left\| \boldsymbol{\xi}_1 \right\|^2 \\ &\quad + \frac{1}{2} \boldsymbol{\xi}_2^{\mathrm{T}} \boldsymbol{\xi}_2 - \boldsymbol{\xi}_2^{\mathrm{T}} \boldsymbol{C}_2 \boldsymbol{\xi}_2 + \boldsymbol{\xi}_2^{\mathrm{T}} \boldsymbol{G} \Delta \boldsymbol{U} + \gamma_1 \tilde{\kappa} \hat{\kappa} \end{aligned} \tag{55}$$

Noting the term $\boldsymbol{\xi}_2^{\mathrm{T}} \boldsymbol{G} \Delta \boldsymbol{U}$ and $\| z_{2i} \| d_m$ in (55), the following inequalities hold

$$\boldsymbol{\xi}_2^{\mathrm{T}} \boldsymbol{G} \Delta \boldsymbol{U} \leq \frac{1}{2} \boldsymbol{\xi}_2^{\mathrm{T}} \boldsymbol{\xi}_2 + \frac{1}{2} \bar{g}^2 \vartheta^2 \tag{56}$$

$$\| z_{2i} \| d_m \leq \frac{\kappa z_{2i}^2}{2\varepsilon^2} + \frac{\varepsilon^2}{2} \tag{57}$$

Then substituting (56) and (57) into (55), we can obtain

$$\begin{aligned}\dot{V}_2 &\leq -\sum_{i=1}^{6} \frac{k_{1i} z_{1i}^2}{b_{1i}^2 - z_{1i}^2} - \sum_{i=1}^{6} \frac{k_{2i} z_{2i}^2}{b_{2i}^2 - z_{2i}^2} \\ &\quad + \sum_{i=1}^{6} \frac{\varepsilon^2 / 2}{b_{2i}^2 - z_{2i}^2} - \bar{C}_1 \left\| \boldsymbol{\xi}_1 \right\|^2 \\ &\quad + \frac{1}{2} \boldsymbol{\xi}_2^{\mathrm{T}} \boldsymbol{\xi}_2 - \boldsymbol{\xi}_2^{\mathrm{T}} \boldsymbol{C}_2 \boldsymbol{\xi}_2 + \frac{1}{2} \boldsymbol{\xi}_2^{\mathrm{T}} \boldsymbol{\xi}_2 + \frac{1}{2} \bar{g}^2 \theta^2 + \gamma_1 \tilde{\kappa} \hat{\kappa} \\ &\leq -\sum_{i=1}^{6} \frac{k_{1i} z_{1i}^2}{b_{1i}^2 - z_{1i}^2} - \sum_{i=1}^{6} \frac{k_{2i} z_{2i}^2}{b_{2i}^2 - z_{2i}^2} \\ &\quad + \sum_{i=1}^{6} \frac{\varepsilon^2 / 2}{b_{2i}^2 - z_{2i}^2} - \bar{C}_1 \left\| \boldsymbol{\xi}_1 \right\|^2 \\ &\quad - \bar{C}_2 \left\| \boldsymbol{\xi}_2 \right\|^2 + \frac{1}{2} \bar{g}^2 \vartheta^2 - \gamma_1 \tilde{\kappa}^2 + \gamma_1 \left(\frac{o}{2} \tilde{\kappa}^2 + \frac{1}{2o} \kappa^2 \right) \end{aligned} \tag{58}$$

where $\bar{C}_2 = \lambda_{\min}(\boldsymbol{C}_2) - 1 > 0$.

In view of Lemma 3, (58) can be further simplified into

$$\begin{aligned}\dot{V}_2 &\leq -\sum_{i=1}^{6} \frac{1}{2} \ln \frac{k_{1i} b_{1i}^2}{b_{1i}^2 - z_{1i}^2} - \sum_{i=1}^{6} \frac{1}{2} \ln \frac{k_{2i} b_{2i}^2}{b_{2i}^2 - z_{2i}^2} - \bar{C}_1 \left\| \boldsymbol{\xi}_1 \right\|^2 \\ &\quad - \bar{C}_2 \left\| \boldsymbol{\xi}_2 \right\|^2 - \gamma_1 \tilde{\kappa}^2 + \sum_{i=1}^{6} \frac{\varepsilon^2 / 2}{b_{2i}^2 - z_{2i}^2} + \frac{1}{2} \bar{g}^2 \vartheta^2 \\ &\quad + \gamma_1 \left(\frac{o}{2} \tilde{\kappa}^2 + \frac{1}{2o} \kappa^2 \right) \\ &\leq -\beta V_2 + C \end{aligned} \tag{59}$$

where

$$\beta = \min\{2\lambda_{\min}(\boldsymbol{K}_1),\ 2\lambda_{\min}(\boldsymbol{K}_2),\ 2\bar{C}_j,\ 2\gamma_0\gamma_1(1-\frac{o}{2}), j=1,2\Big\},$$

$$C = \sum_{i=1}^{6}\frac{\varepsilon^2/2}{b_{2i}^2 - z_{2i}^2} + \frac{1}{2}\bar{g}^2\vartheta^2 + \gamma_1\left(\frac{o}{2}\tilde{\kappa}^2 + \frac{1}{2o}\kappa^2\right).$$

According to Lemma 1, if the initial conditions are satisfied, then $|z_{1i}| < b_{1i}$, $|z_{2i}| < b_{2i}$ hold for any $t > 0$. Furthermore, from Lemma 2, we have $z_{1i}, z_{2i}, \tilde{\kappa}, \xi_{1i}, \xi_{2i} (i = 1, \ldots, 6)$ are all bounded. Defining $\|\xi_{1i}\| \le \delta_{1i}$, $\|\xi_{2i}\| \le \delta_{2i}$, then $|x_{1i}| = |z_{1i} + \xi_{1i} + x_{di}| < b_{1i} + \delta_{1i} + A_{0i}b_{ai}$ and $|x_{2i}| = |z_{2i} + \xi_{2i} + \alpha_i + \dot{x}_{di}| < b_{2i} + \delta_{2i} + k_{1i}b_{1i} + A_{1i}b_{ci}$ hold. Integrating the inequality (59), we can obtain

$$0 \le V_2(t) \le \left(V_2(0) - \frac{C}{\beta}\right)e^{-\beta t} + \frac{C}{\beta} \le V_2(0) + \frac{C}{\beta} \tag{60}$$

In the view of the definition of V_2, we get

$$\frac{1}{2}\ln\frac{b_{1i}^2}{b_{1i}^2 - z_{1i}^2} \le V_2(0) + \frac{C}{\beta} \tag{61}$$

Taking exponentials on both sides of (61) yields

$$|z_{1i}| \le b_{1i}\sqrt{1 - e^{-2(V_2(0)+C/\beta)}} \le b_{1i}, \quad \forall t > 0 \tag{62}$$

Similarly, for z_2, there is $|z_{2i}| \le b_{2i}\sqrt{1 - e^{-2(V_2(0)+C/\beta)}} \le b_{2i}$, $\forall t > 0$. Hence, we can choose appropriate controller parameters that the state error z_1, z_2 finally converge to any a small neighborhood of zero. This completes the proof of **Theorem 2**.

Remark 7: Note that the anti-windup auxiliary subsystem (44) is a linear bounded-input, bounded-output (BIBO) system. Theorem 2 implies that the state of auxiliary system $\boldsymbol{\xi}_1$, $\boldsymbol{\xi}_2$ are all uniformly ultimately bounded, meaning $\Delta\boldsymbol{U}$ is also bounded, and explaining the rationality of Assumption 4 from another perspective.

Remark 8: From **Theorem 2**, we can obtain both the satisfactory steady accuracy and appropriate transient performance by choosing the controller parameters. For example, the response rate will be accelerated by increasing $\boldsymbol{K}_1$, while introducing unexpected noises into the closed-loop system. Similarly, increasing $\boldsymbol{K}_2$ will also enhance the noises. However, the convergence rate will be much slower if $\boldsymbol{K}_1$, $\boldsymbol{K}_2$ are chosen as too small value. Hence, the advantages and disadvantages must be weighed, and the two aspects taken into consideration when adjusting the parameters. Furthermore, $\boldsymbol{C}_1$ and $\boldsymbol{C}_2$ are the negative feedback gain matrices of auxiliary subsystem (44), so it is important that the conditions $\lambda_{\min}(\boldsymbol{C}_1) - 1/2 > 0$ and $\lambda_{\min}(\boldsymbol{C}_2) - 1 > 0$ are satisfied to guarantee the stability of the closed-loop system.

IV. SIMULATIONS AND ANALYSES

In this section, numerical simulations are conducted to evaluate the performance of the proposed controllers.

TABLE 1. System parameters and initial conditions.

Parameters	Value
$\rho(0)$	10 m
$q_\varepsilon(0)$	0.9rad
$q_\beta(0)$	−1.8rad
ρ_d	2 m
$\boldsymbol{\Omega}(0)$	$[-0.3, -0.9, 2.7]^{\mathrm{T}}$ rad
$\boldsymbol{J}_s$	$\mathrm{diag}(30, 25, 20)\mathrm{kg}\cdot\mathrm{m}^2$

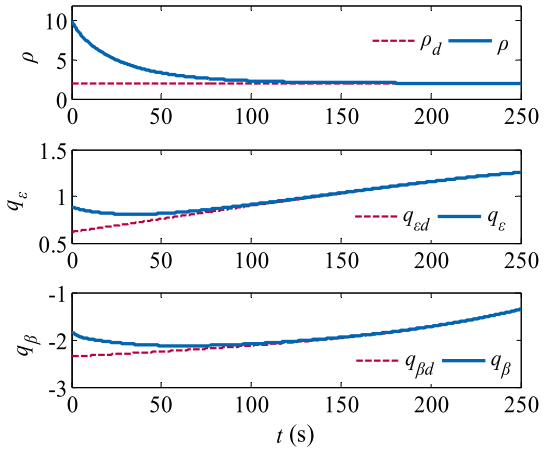

FIGURE 5. Relative position tracking trajectory under controller (29).

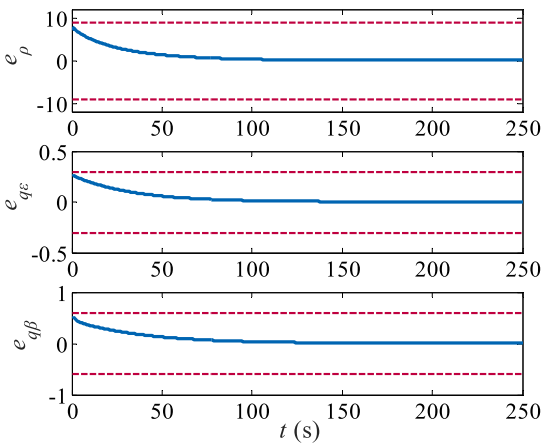

FIGURE 6. Relative position tracking error under controller (29).

A. SIMULATION CONDITIONS AND CONTROLLER PARAMETERS

The initial relative position, attitude, and system parameters are summarized in Table. 1.

As shown in Table. 1, the servicer is assumed to have an initial relative position and attitude $\rho(0)$, $q_\varepsilon(0)$, $q_\beta(0)$ and $\boldsymbol{\Omega}(0)$. Additionally, the initial orbital elements of the target is $a = 42241$km, $e = 0$, $i = 0°$, $\omega = 0°$, $\Omega = 0°$, and $f = 0°$. The initial body frame of the target

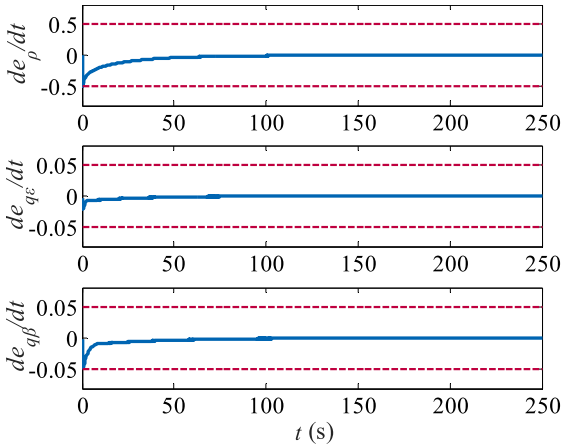

FIGURE 7. Relative velocity tracking error under controller (29).

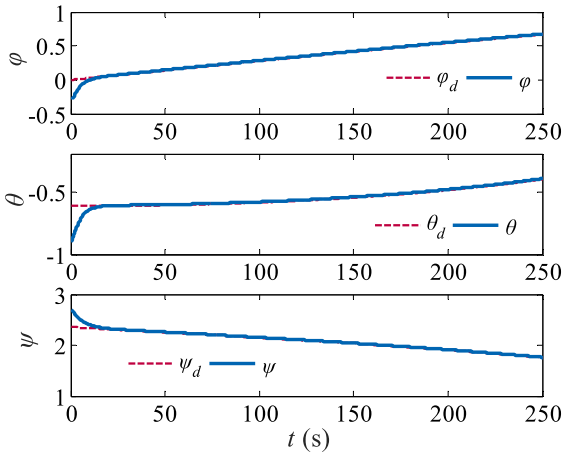

FIGURE 8. Attitude tracking trajectory under controller (29).

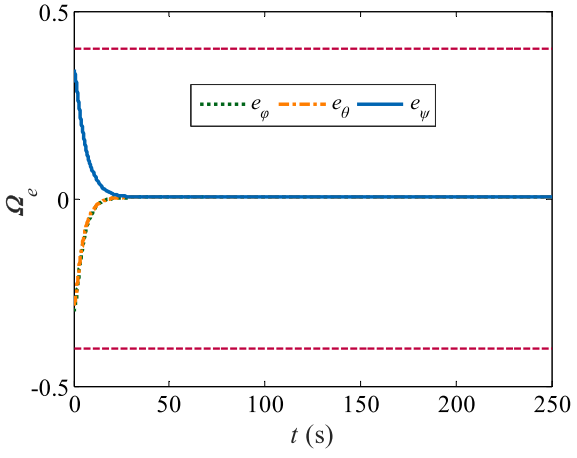

FIGURE 9. Attitude tracking error under controller (29).

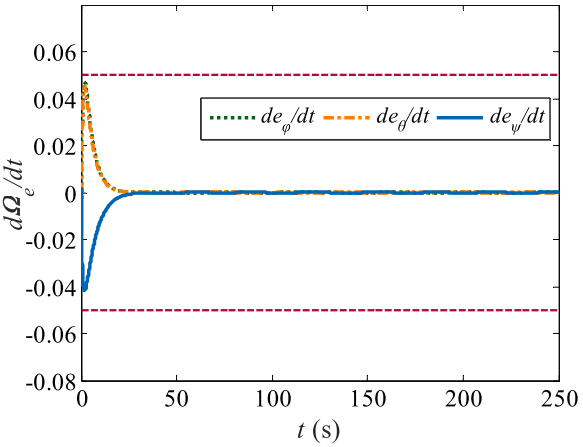

FIGURE 10. Angular velocity tracking error under controller (29).

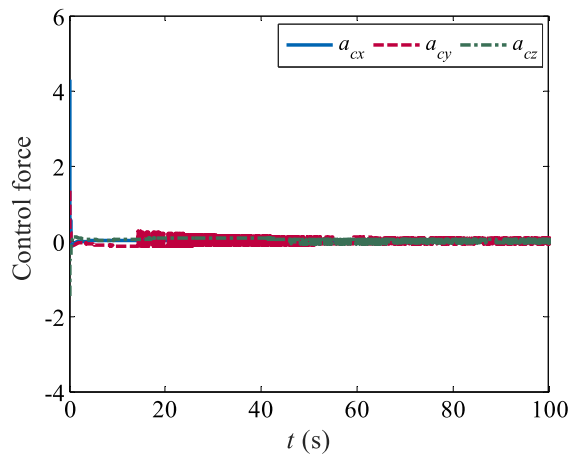

FIGURE 11. Control force under controller (29).

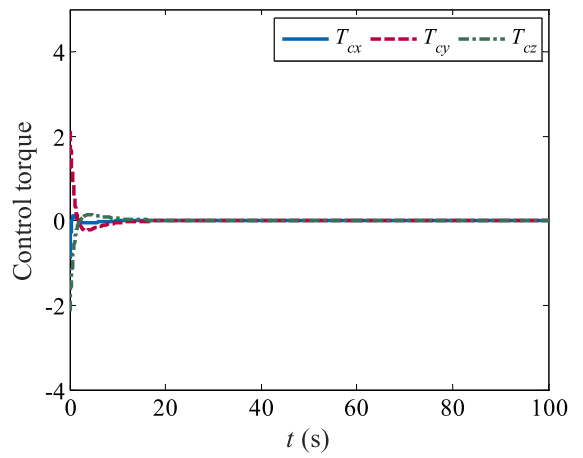

FIGURE 12. Control torque under controller (29).

is coincident with C_i, and its angular velocity expressed in its body frame is $[-0.0020.002 - 0.002]^T$ rad/s. The unit vector of the feature points in the target's body frame is $\boldsymbol{n}_b = [\sqrt{3}/3, -\sqrt{3}/3, -\sqrt{3}/3]^T$, and the sunlight vector expressed in C_l is $\boldsymbol{\mathcal{O}} = [-\sqrt{3}/3, \sqrt{3}/3, -\sqrt{3}/3]^T$. The disturbances effect on the servicer are:

$$\boldsymbol{a}_d = \begin{bmatrix} 2\cos(0.015t) \\ \sin(0.01t) \\ 1.5\cos(0.02t) \end{bmatrix} \times 10^{-2}\ \mathrm{m/s^2},$$

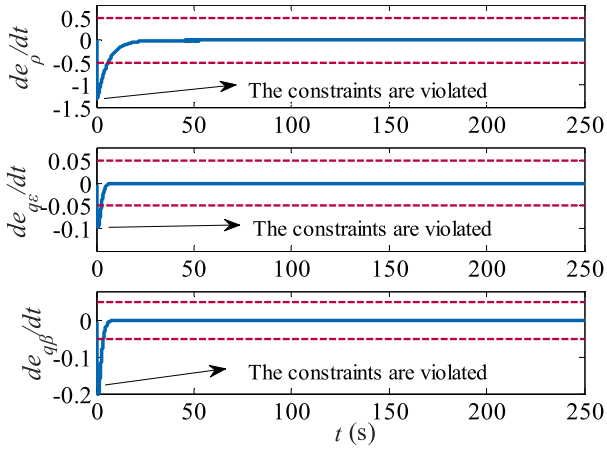

FIGURE 13. Relative velocity tracking error under controller (35).

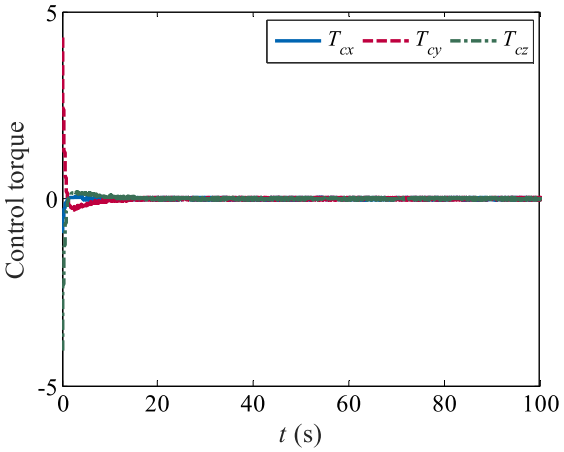

FIGURE 16. Control torque under controller (35).

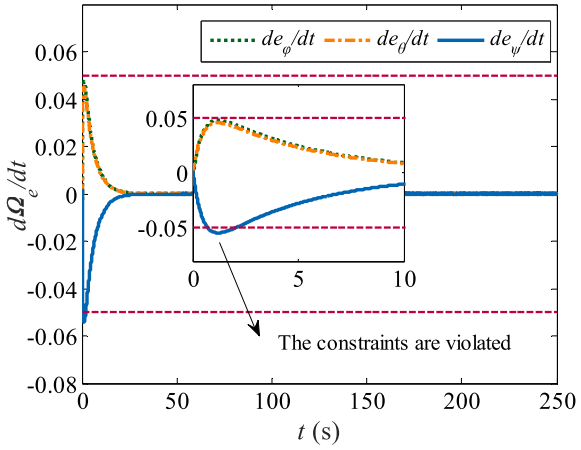

FIGURE 14. Angular velocity tracking error under controller (35).

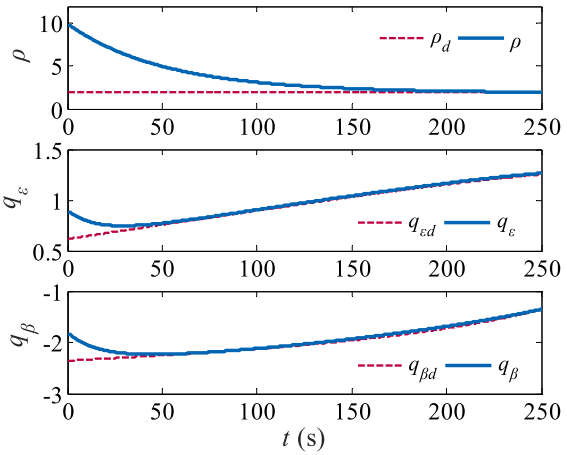

FIGURE 17. Relative position tracking trajectory under controller (51).

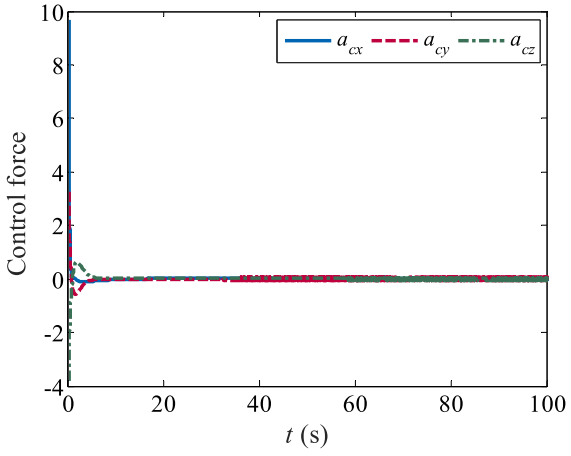

FIGURE 15. Control force under controller (35).

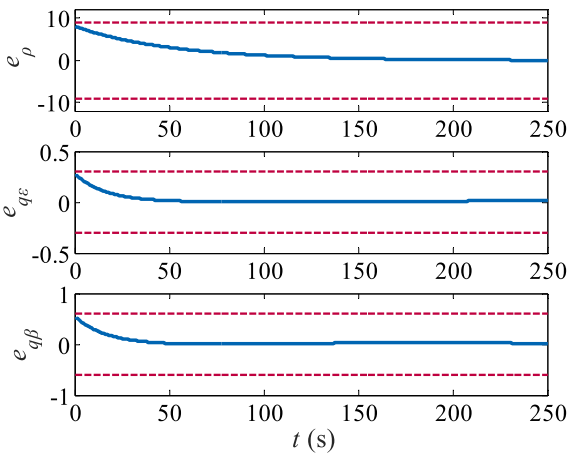

FIGURE 18. Relative position tracking error under controller (51).

$$\boldsymbol{T}_d = \begin{bmatrix} 2\cos(0.015t) \\ \sin(0.01t) \\ 1.5\cos(0.02t) \end{bmatrix} \times 10^{-3}\ \mathrm{N}\cdot\mathrm{m}$$

For the fairness of comparison, the full-state constraints, input constraints, and controller parameters are the same for the following simulation study. During the final approaching stage of a rendezvous, the system errors are constrained by $\boldsymbol{b}_1 = \mathrm{diag}(9, 0.3, 0.6, 0.4, 0.4, 0.4)$, $\boldsymbol{b}_2 = \mathrm{diag}(0.5, 0.05, 0.05, 0.05, 0.05, 0.05)$. The controller parameters are $\boldsymbol{K}_1 = \mathrm{diag}(0.03, 0.03, 0.025, 0.2, 0.2, 0.2)$,

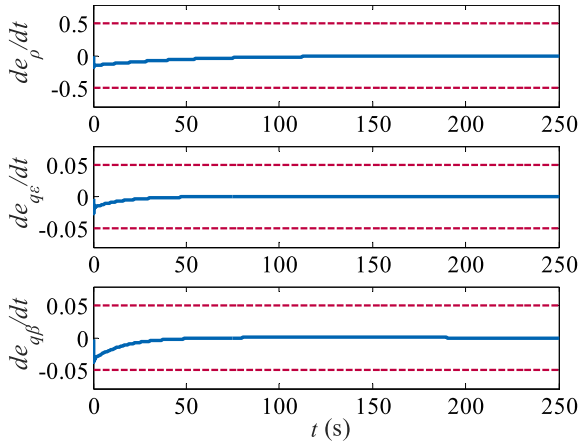

FIGURE 19. Relative velocity tracking error under controller (51).

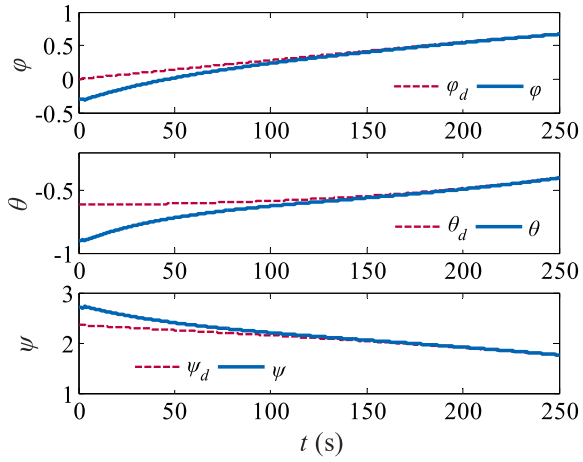

FIGURE 20. Attitude tracking trajectory under controller (51).

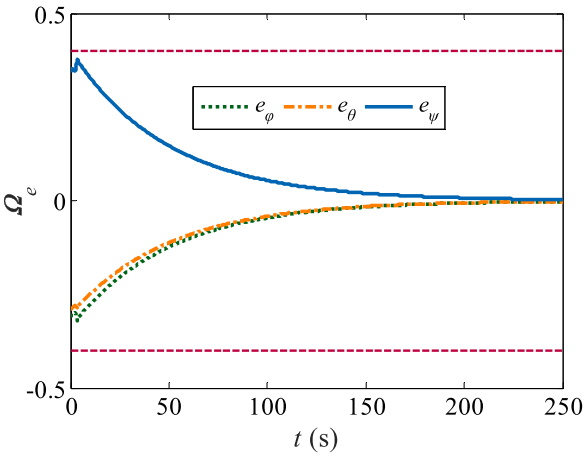

FIGURE 21. Attitude tracking error under controller (51).

$\boldsymbol{K}_2 = \text{diag}(5.5, 3, 3, 2.6, 2.6, 2.6)$, $\gamma_0, \gamma_1 = 0.01$, $\boldsymbol{C}_1 = 20\boldsymbol{I}_6$, $\boldsymbol{C}_2 = 50\boldsymbol{I}_6$. The control force and torque are restricted by 1 m/s^2 and 2 N $\cdot$ m.

B. RESULT ANALYSIS

The 6-DOF tracking trajectory and tracking error under the proposed controller (29) are depicted in Figs. 5-10, respectively. As shown in Fig. 5 and Fig. 8, the relative position and attitude tracking with the controller (29) can be achieved within 175s and 20s, respectively. We can see that the Lyapunov stability of the closed-loop system is guaranteed, and the system state asymptotically converges into a small neighborhood of zero. From Fig. 6, 7, 9 and 10, it can be

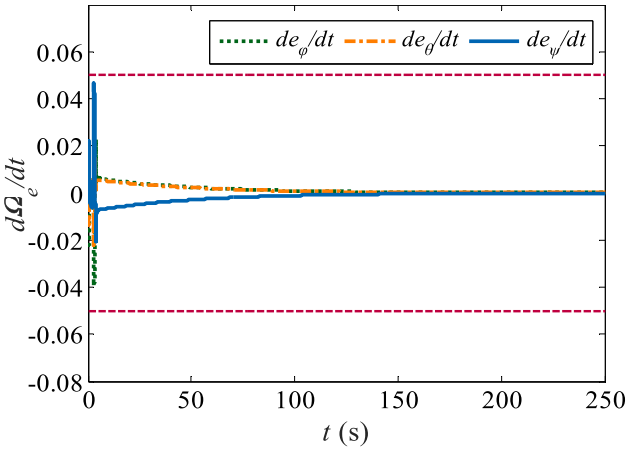

FIGURE 22. Angular velocity tracking error under controller (51).

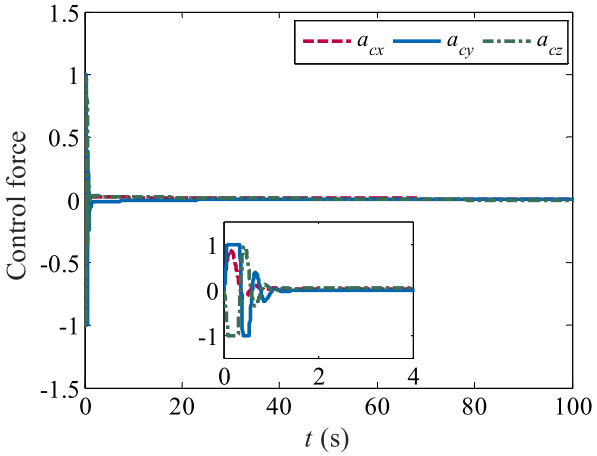

FIGURE 23. Control force under controller (51).

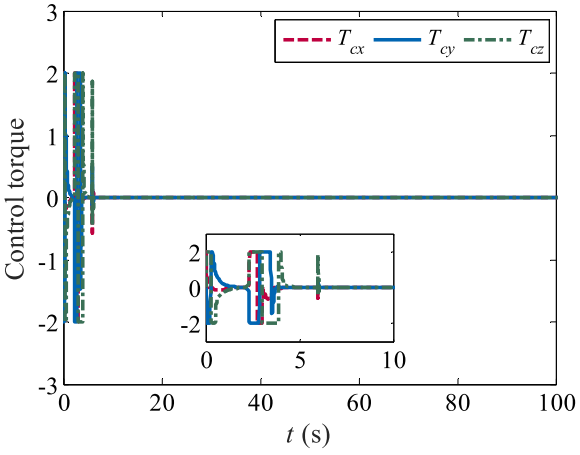

FIGURE 24. Control torque under controller (51).

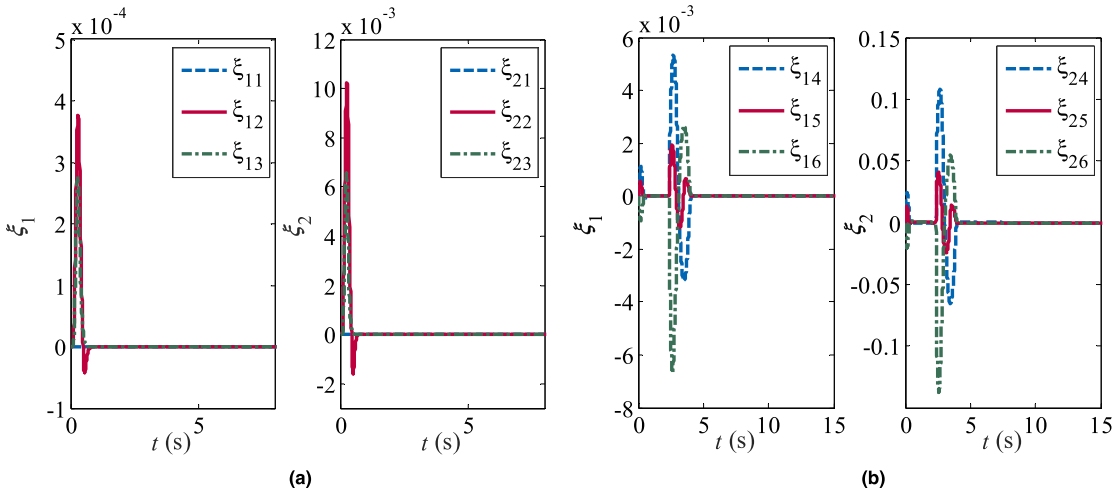

FIGURE 25. The output signals ξ_1 and ξ_2 of the anti-windup auxiliary subsystem (44).

determined that the bounds for the closed-loop error signals are never violated during the entire dynamic process.

The time responses of control force and torque are curved in Fig. 11 and 12. Due to the existence of initial state error, the maximum control inputs are 4.5m/s^2 and 2.5N$\cdot$m, respectively. Along with the convergence of all the states to desired values, the control inputs decrease gradually. Furthermore, the chattering phenomenon is obviously existed in the time responses of control force, even after the system states have tracked with the desired ones. The direct reason is the existence of sign function in the controller (29).

To illustrate the restrictive condition given in *Remark. 4*, here Figs. 13-16 display the simulation results of conventional quadratic Lyapunov-based controller (35).

It is obvious that the initial conditions given in Table 1 do not satisfy the condition (39). Hence, comparing the simulation results of the two controllers based on Barrier Lyapunov and quadratic Lyapunov function, it can be concluded that:

a. Both two controllers (29) and (35) can ensure the convergence of relative position and attitude to the desired value and quadratic Lyapunov based method has a faster convergence rate and less settling time.

b. Although quadratic Lyapunov based method has a better transient performance, the second order states (curved in Fig. 13 and Fig. 14) violate the prescribed bound distinctly with the same initial conditions as BLF method. In contrast, BLF method could ensure boundness of the full state in the constraints during the entire dynamic process.

Figs. 17-25 describe the simulation results of controller (51) with adaptive law (52). The time responses of relative position, attitude, and the state error are depicted in Figs. 17-22. It can be observed that the Lyapunov stability of the closed-loop system is ensured with input and full-state constraints, and all system states never violate the prescribed bound during the entire dynamic process. Obviously, the proposed control scheme still has a good tracking performance, even if the physical conditions limit the maximum input. This implies that the developed adaptive control scheme is valid for the 6-DOF spacecraft system with external disturbances, and multiple physical constraints.

As a comparison of Figs. 11-12 and Figs. 15-16, in which the chattering phenomenon is distinctly existed, the time responses of control force and torque under controller (51) are shown in Figs. 23-24. We can see that the proposed controller (51) with adaptive law (52) is fundamentally smooth without a sign function Moreover, it can be further observed that the control force and torque achieve the bound of saturation with 1m/s^2 and 2N $\cdot$ m, and the tracking control performance still remains good. The reason is that the control command calculated by controller (51) overtops the input constraints, and the excess part is compensated by the term $\boldsymbol{C}_2\boldsymbol{\xi}_2$ to guarantee the stability. As depicted in Fig. 25, the output signals of the auxiliary subsystem are bounded, so all the signals of the closed-loop system are ultimately bounded. Hence, summarizing the simulation results, we can conclude that the 6-DOF final approaching task of a rendezvous is achieved under multiple physical constraints with a satisfactory tracking performance.

V. CONCLUSIONS

This paper focuses on the 6-DOF tracking control problem for a noncooperative space target in the final approaching stage of a rendezvous task, in which external disturbances, model uncertainties, input and full-state constraints are taken into accounted simultaneously. Two 6-DOF integrated tracking controllers are developed to address and overcome the full-state constraints explicitly with the Barrier Lyapunov Function technique. Moreover, the novel adaptive controller with input and full-state constraints is smooth by estimating the square of unknown upper bound of disturbances and uncertainties. This result provides a new insight into the 6-DOF integrated tracking control and has potential benefits for on-orbit services, since the relative position and

attitude constraints are strictly guaranteed and chattering phenomenon is effectively avoided. The performance of the proposed controllers is further illustrated by numerical simulation examples. In our further research, more practical situations will be taken into consideration such as control allocation, actuator faults, and collision avoidance.

REFERENCES

[1] A. Long, M. Richards, and D. E. Hastings, "On-orbit servicing: A new value proposition for satellite design and operation," *J. Spacecraft Rockets*, vol. 44, pp. 964–976, 2007.
[2] W. Xu, B. Liang, C. Li, and Y. Xu, "Autonomous rendezvous and robotic capturing of non-cooperative target in space," *Robotica*, vol. 28, no. 5, pp. 705–718, 2009.
[3] P. K. C. Wang, F. Y. Hadaegh, and K. Lau, "Synchronized formation rotation and attitude control of multiple free-flying spacecraft," *J. Guid., Control, Dyn.*, vol. 22, no. 1, pp. 28–35, 1999.
[4] R. Kristiansen, P. J. Nicklasson, and J. T. Gravdahl, "Spacecraft coordination control in 6DOF: Integrator backstepping vs passivity-based control," *Automatica*, vol. 44, no. 11, pp. 2896–2901, Nov. 2008.
[5] K. Subbarao and S. Welsh, "Nonlinear control of motion synchronization for satellite proximity operations," *J. Guid., Control, Dyn.*, vol. 31, no. 5, pp. 1284–1294, 2008.
[6] Q. Lan, J. Yang, S. Li, and H. Sun, "Finite-time control for 6DOF spacecraft formation flying systems," *J. Aerosp. Eng.*, vol. 28, no. 5, 2015, Art. no. 04014137.
[7] J. Zhang, Z. Sun, M. Liu, and D. Ye, "6-DOF coupled spacecraft tracking control via adaptive fuzzy technique," in *Proc. 4th Int. Conf. Inf., Cybern. Comput. Social Syst.*, Dalian, China, Jul. 2017, pp. 484–489.
[8] Y. Li, Z. Jing, and S. Hu, "Dynamic optimal sliding-mode control for six-DOF follow-up robust tracking of active satellite," *Acta Astronaut.*, vol. 69, nos. 7–8, pp. 559–570, 2011.
[9] M. Xin and H. Pan, "Integrated nonlinear optimal control of spacecraft in proximity operations," *Int. J. Control*, vol. 83, no. 2, pp. 347–363, Mar. 2010.
[10] S. Di Cairano, H. Park, and I. Kolmanovsky, "Model predictive control approach for guidance of spacecraft rendezvous and proximity maneuvering," *Int. J. Robust Nonlinear Control*, vol. 22, no. 12, pp. 1398–1427, 2012.
[11] W. H. Clohessy and R. S. Wiltshire, "Terminal guidance system for satellite rendezvous," *J. Aerosp. Sci.*, vol. 27, no. 9, pp. 653–658, Jan. 1960.
[12] D. F. Lawden, *Optimal Trajectories for Space Navigation*. London, U.K.: Butterworths, 1963, pp. 79–86.
[13] X. Gao, K. L. Teo, and G.-R. Duan, "Robust $H\infty$ control of spacecraft rendezvous on elliptical orbit," *J. Franklin Inst.*, vol. 349, no. 8, pp. 2515–2529, 2012.
[14] D. Zhang, J. Luo, D. Gao, W. Ma, and J. Yuan, "A novel nonlinear control for tracking and rendezvous with a rotating non-cooperative target with translational maneuver," *Acta Astronautica*, vol. 138, pp. 276–289, Sep. 2017.
[15] T. Chen and S. Xu, "Double line-of-sight measuring relative navigation for spacecraft autonomous rendezvous," *Acta Astronautica*, vol. 67, nos. 1–2, pp. 122–134, 2010.
[16] W. Wang, L. Chen, K. Li, and Y. Lei, "One active debris removal control system design and error analysis," *Acta Astronaut.*, vol. 128, pp. 499–512, Nov./Dec. 2016.
[17] L. Sun, W. Huo, and J. Xia, "Robust nonlinear adaptive relative pose control for cooperative spacecraft during rendezvous and proximity operations," *IEEE Trans. Control Syst. Technol.*, vol. 25, no. 5, pp. 1840–1847, Sep. 2017.
[18] Y. Lv, Q. Hu, G. Ma, and J. Zhou, "6 DOF synchronized control for spacecraft formation flying with input constraint and parameter uncertainties," *ISA Trans.*, vol. 50, no. 4, pp. 573–580, 2011.
[19] X. Liu, P. Zhang, K. Liu, and Y. Li, "Compensator-based 6-DOF control for probe asteroid-orbital-frame hovering with actuator limitations," *Adv. Space Res.*, vol. 57, no. 9, pp. 1914–1927, 2016.
[20] L. Sun and Z. Zheng, "Disturbance observer-based robust saturated control for spacecraft proximity maneuvers," *IEEE Trans. Control Syst. Technol.*, vol. 26, no. 2, pp. 684–692, Mar. 2018.
[21] F. Zhang and G. Duan, "Robust adaptive integrated translation and rotation control of a rigid spacecraft with control saturation and actuator misalignment," *Acta Astronautica*, vol. 86, pp. 167–187, Mar. 2013.
[22] Y. Cheng, D. Ye, Z. Sun, and S. Zhang, "Spacecraft reorientation control in presence of attitude constraint considering input saturation and stochastic disturbance," *Acta Astronautica*, vol. 144, pp. 61–68, Mar. 2018.
[23] D. Li, G. Ma, C. Li, W. He, J. Mei, and S. S. Ge, "Distributed attitude coordinated control of multiple spacecraft with attitude constraints," *IEEE Trans. Aerosp. Electron. Syst.*, vol. 54, no. 5, pp. 2233–2245, Oct. 2018.
[24] A. Weiss, M. Baldwin, R. S. Erwin, and I. Kolmanovsky, "Model predictive control for spacecraft rendezvous and docking: Strategies for handling constraints and case studies," *IEEE Trans. Control Syst. Technol.*, vol. 23, no. 4, pp. 1638–1647, Jul. 2015.
[25] X. Jin, "Nonrepetitive leader–follower formation tracking for multiagent systems with LOS range and angle constraints using iterative learning control," *IEEE Trans. Cybern.*, vol. 49, no. 5, pp. 1748–1758, May 2019.
[26] L. Sun, W. Huo, and Z. Jiao, "Adaptive backstepping control of spacecraft rendezvous and proximity operations with input saturation and full-state constraint," *IEEE Trans. Ind. Electron.*, vol. 64, no. 1, pp. 480–492, Jan. 2017.
[27] K. P. Tee, S. S. Ge, and E. H. Tay, "Barrier Lyapunov functions for the control of output-constrained nonlinear systems," *Automatica*, vol. 45, no. 4, pp. 918–927, Apr. 2009.
[28] B. Ren, S. S. Ge, K. P. Tee, and T. H. Lee, "Adaptive neural control for output feedback nonlinear systems using a barrier Lyapunov function," *IEEE Trans. Neural Netw.*, vol. 21, no. 8, pp. 1339–1345, Aug. 2010.
[29] Z. Zhao, W. He, and S. S. Ge, "Adaptive neural network control of a fully actuated marine surface vessel with multiple output constraints," *IEEE Trans. Control Syst. Technol.*, vol. 22, no. 4, pp. 1536–1543, Jul. 2014.
[30] Q. Hu and X. Shao, "Smooth finite-time fault-tolerant attitude tracking control for rigid spacecraft," *Aerosp. Sci. Technol.*, vol. 55, pp. 144–157, Aug. 2016.

YUHAN LIU received the B.S. and M.Sc. degrees in control science and engineering from the Harbin Institute of Technology, Harbin, China, in 2015 and 2017, respectively, where she is currently pursuing the Ph.D. degree in control science and engineering.

Her current research interests include spacecraft control, adaptive control, and nonlinear control.

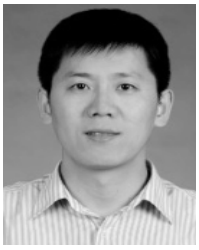

YUEYONG LYU received the B.S. and M.Sc. degrees in automation and the Ph.D. degree in control science and engineering from the Harbin Institute of Technology, Harbin, China, in 2006, 2008, and 2012, respectively.

He is currently an Assistant Researcher with the Department of Astronautics, Harbin Institute of Technology, where he performs research in the fields of nonlinear control, satellite attitude control, and formation flying.

GUANGFU MA received the M.Sc. and Ph.D. degrees in electrical engineering from the Harbin Institute of Technology, in 1993 and 1987, respectively.

He joined the Harbin Institute of Technology as an Associate Professor, in 1992, and as a Professor, in 1997, where he teaches and performs research in the fields of nonlinear control, satellite attitude control, and formation flying, and is currently a Professor with the Department of Control Science and Engineering.